Nuclear Mathematical and Computational Sciences: A Century in Review, A Century Anew
Gatlinburg, Tennessee, April 6-11, 2003, on CD-ROM, American Nuclear Society, LaGrange Park, IL (2003)

ON THE USE OF BIASED ANGULAR QUADRATURE FORMULAS FOR THE NUMERICAL TREATMENT OF PARTICLE TRANSPORT IN MEDIA WITH HIGHLY FORWARD-PEAKED SCATTERING

Richard Sanchez
Direction de l'Energie Nucléaire
Service des Etudes de Réacteurs et de Modélisation Avancée
CEA de Saclay, DM2S/SERMA
91191 Gif-sur-Yvette cedex, France
richard.sanchez@cea.fr

Norman J. McCormick
Department of Mechanical Engineering
University of Washington
Seattle, WA 98195
mccor@u.washington.edu

ABSTRACT

The use of biased angular quadrature formulas in conjunction with source evaluation from cell-averaged angular fluxes is investigated to increase the precision of the angular representation and to reduce memory requirements for the discrete ordinates solution of highly forward-peaked scattering (HFPS) problems. Also, a twice-collided source is introduced to avoid numerical representation of singularities in the solution. As an example calculation the propagation and spreading of a collimated particle beam in a HFPS medium has been calculated with a discrete ordinates diamond-differenced numerical solution of the transport equation in two-dimensional curvilinear cylindrical coordinates. The calculation was carried out for a strongly forward-peaked Henyey-Greenstein scattering law for which Fokker-Plank asymptotic models are not valid. The results show promise for numerically calculated reference solutions based on accurate spatial representations for checking the accuracy of standard asymptotic models used for these types of problems.

Key Words: Transport, Angular Quadrature, Forward-Peaked Scattering, Henyey-Greenstein

1. INTRODUCTION

In this work we consider one-group linear particle transport in isotropic media with collisions characterized by a highly forward-peaked scattering kernel $f_{scat}(\mathbf{r}, \mathbf{\Omega} \cdot \mathbf{\Omega}')$ that we take normalized to 1,

$$\int_{(4\pi)} d\mathbf{\Omega}' f_{scat}(\mathbf{r}, \mathbf{\Omega} \cdot \mathbf{\Omega}') = 1, \tag{1}$$

where $\mathbf{\Omega}$ is the initial particle direction and $\mu_{coll} = \mathbf{\Omega} \cdot \mathbf{\Omega}'$ is the cosine of the angle between the initial direction of the particle $\mathbf{\Omega}$ and its direction after collision $\mathbf{\Omega}'$. The scattering kernel is the density of probability for the direction $\mathbf{\Omega}'$ or, properly renormalized, the density of probability for μ_{coll} and, as such, can be characterized by a complete set of statistical moments (the mean $\overline{\mu}_{coll}$, the variance σ^2, etc.) However, for applications to particle transport it is convenient to take advantage of the invariance of the kernel with respect to orthogonal transformations (rotations and symmetries) and introduce an expansion in terms of Legendre polynomials,

$$f_{scat}(\mathbf{r}, \mathbf{\Omega} \cdot \mathbf{\Omega}') = \frac{1}{4\pi} \sum_{k=0}^{K_{scat}} (2k+1) f_k(\mathbf{r}) P_k(\mathbf{\Omega} \cdot \mathbf{\Omega}'), \tag{2}$$

where

$$f_k(\mathbf{r}) = \int_{(4\pi)} d\mathbf{\Omega}' f_{scat}(\mathbf{r}, \mathbf{\Omega} \cdot \mathbf{\Omega}') P_k(\mathbf{\Omega} \cdot \mathbf{\Omega}')$$

with, in particular, $1 = f_0$, $\overline{\mu}_{coll} = f_1$ and $\sigma^2 = (2/3) f_2 - f_1^2 + 1/3$.

Although the expansion in Legendre polynomials should be taken all the way to infinity, in practice a truncation is done at some finite order K_{scat} for which higher-order coefficients are small enough that their sum can be neglected. By highly forward-peaked scattering (HFPS) we understand here a scattering kernel with a mean collision cosine $\overline{\mu}_{coll}$ very near 1, requiring hundreds or even thousands of terms in expansion (2). The physics of HFPS is that of particles undergoing collisions involving very small momenta exchanges so that, on the average, a particle has to go through many collisions to deviate appreciably from its initial direction. Problems with HFPS occur in many areas of particle transport whenever there is propagation in a HFPS medium of particles emitted from localized sources; this includes charged particle (e.g., electron) transport, photon transport in the atmosphere or in sea waters, and medical (e.g., electron or ion therapy) applications, among others. One of the more challenging questions in HFPS transport is the prediction of the transverse dispersion of a collimated beam as it propagates in a HFPS medium. Generally, HFPS problems involve the energy variable as well and are also characterized by very small losses of energy per collision event. However, in this work we have exclusively considered the one-group problem by assuming that the energy has properly been taken care of by a suitable slowing-down model or a multigroup approximation.

Perhaps the earliest work on beam dispersion was presented by Fermi in a seminar given in 1940 at the University of Chicago and published a year later by Rossi and Greisen.[1] The Fermi-Eyges solution belongs to a family of asymptotic models for the transport equation collectively known as the Fokker-Planck approximations. The basic idea behind these models is to use the fact that $\overline{\mu}_{coll} \sim 1$ to derive a simplified transport equation in the limit $\overline{\mu}_{coll} \longrightarrow 1$. Roughly, one introduces a limited Taylor expansion of the radiation field around $\mathbf{\Omega}' \approx \mathbf{\Omega}$ which results in the replacement of the integral collision operator,

$$(Hf)(\mathbf{r}, \mathbf{\Omega}) = \int_{(4\pi)} d\mathbf{\Omega}' \Sigma_s(\mathbf{r}, \mathbf{\Omega}' \cdot \mathbf{\Omega}) f(\mathbf{r}, \mathbf{\Omega}') \tag{3}$$

with kernel $\Sigma_s(\mathbf{r}, \mathbf{\Omega} \cdot \mathbf{\Omega}') = \Sigma_s(\mathbf{r}) f_{scat}(\mathbf{r}, \mathbf{\Omega} \cdot \mathbf{\Omega}')$, by an approximate differential operator. The resulting Fokker-Planck equation depends on how many terms are used in the expansion. The lowest approximation for the angular flux ψ, $\psi(\mathbf{r}, \mathbf{\Omega}') \sim \psi(\mathbf{r}, \mathbf{\Omega})$, is equivalent to replacing $f_{scat}(\mathbf{r}, \mathbf{\Omega} \cdot \mathbf{\Omega}')$ with Plazcek's delta

function[2] on the surface of the unit sphere, $\delta_2(\mathbf{\Omega}\cdot\mathbf{\Omega}')$, and results in a collisionless transport equation with the total cross section replaced by the absorption cross section, $\Sigma(\mathbf{r}) \longrightarrow \Sigma(\mathbf{r}) - \Sigma_s(\mathbf{r})$. The next-order approximation that consists of retaining terms up to second order yields the well-known Fokker-Planck collision operator,[3]

$$(H_{FP}\psi)(\mathbf{r},\mathbf{\Omega}) = \frac{\Sigma_{tr}(\mathbf{r})}{2}(\triangle\psi)(\mathbf{r},\mathbf{\Omega}),$$

where $\Sigma_{tr}(\mathbf{r}) = \Sigma(\mathbf{r})[1-\overline{\mu}_{coll}(\mathbf{r})]$ is the transport cross section and $\triangle$ is the Laplacian on the surface of the unit sphere.

In the last years a large body of work has been done on extensions of Fermi's results and on the analysis and generalization of the Fokker-Planck equation. Pomraning[4] was the first to carry out a correct asymptotic analysis and to show that the Fokker-Planck equation is formally an asymptotic limit of the transport equation when the total cross section increases to infinity and the average collision cosine goes to one, while the transport-corrected cross section remains finite and bounded from zero:

$$\Sigma \to \infty,\ \overline{\mu}_{coll} \longrightarrow 1,\ 0 < \Sigma_{tr} < \infty.$$

The picture is that Fokker-Planck becomes a valid approximation of transport at the limit when particles undergo an ever increasing number of collisions while each collision deflects the particle less and less. However, as shown by Pomraning, these conditions are necessary but not sufficient. A final constraint is that the scattering kernel has to fall off fast enough as μ_{coll} decreases from its value at 1. In particular, Pomraning showed that the Henyey-Greenstein model,[5] one of the most widely used scattering kernel models, did not decrease fast enough and that, therefore, the Fokker-Planck equation was not the asymptotic limit of the transport equation with a Henyey-Greenstein collision kernel. Soon after, Börgers and Larsen[6] used an elegant mathematical argument to show that the fall condition could be written in the form

$$\frac{\sigma^2}{1-\overline{\mu}_{coll}} \to 0,$$

where we recall that σ^2 denotes the variance of the probability density for μ_{coll}. These authors checked that the condition was not fulfilled by the Henyey-Greenstein model and that it was barely satisfied by screened Rutherford scattering as well as by related elastic scattering models for charged particle transport, results that put strong doubts on the precision of the Fokker-Planck equation for these types of scattering kernels.

Pomraning and co-workers relaxed Fermi's assumptions and derived closed-form solutions for more general regimes including Henyey-Greenstein scattering,[7] large-parameter screened Rutherford scattering[8] and non Fokker-Planck treatments for the beam problem.[9] Pomraning[10] formally generalized his initial asymptotic analysis to an arbitrary order and proposed high-order Fokker-Planck equations. Leakeas and Larsen[11] showed that the eigenvalues of the second-order Fokker-Planck operator proposed by Pomraning become unbounded as $K_{scat} \to \infty$, thus limiting the application of the second-order equation to initial data that are very smooth in angle. In the same work they proposed a corrected high-order Fokker-Planck operator that has the same asymptotic order as the one proposed by Pomraning, preserves the lowest three eigenvalues, and has bounded eigenvalues.

What comes out of all this work is that Fokker-Planck models cannot cope with a general scattering kernel. Another problem with asymptotic models, whether they are Fokker-Planck or not, is that the solution does

not come with useful information for the asymptotic error and one does not even have error bands with respect to the exact solution from the transport equation. Possibly one could go to the next asymptotic order to get an error estimate, but higher-order asymptotic equations either are difficult to solve or they result in unstable solutions.

We present in this work a direct numerical evaluation of the transverse dispersion of a beam in a HFPS medium based on the discrete ordinates approximation and the well-known diamond approximation. The discrete ordinates method has been applied to problems with HFPS and, in particular, to the solution of the Fokker-Planck equation. Good results for angle-integrated quantities were reported by Morel[12],[13] when solving the Fokker-Planck equation in one-dimensional geometries.

A particular difficulty in the application of most discrete ordinates schemes to the treatment of HFPS problems arises from the use of two angular representations: angular fluxes are computed for a finite set of prescribed angular directions (collocation scheme), while angular sources are expressed in a spherical harmonic basis. In the terminology of Morel[14] and Pautz and Adams[15] this requires the use of a moments-to-discrete operator, M, to compute the source for each cell and angular direction during the iteration, and of a discrete-to-moments operator, D, that generates the new source on the harmonic basis at the end of the iteration. As discussed by these authors, the different angular representation used for these two operations may prevent the discrete ordinates approximation from having an asymptotic Fokker-Planck type of limit when the continuous equation has such a limit. This happens whenever the two angular representations are not consistent with each other. Pautz and Adams[15] showed that if the condition $MD \equiv 1$ is satisfied and the original transport equation has a Fokker-Planck limit, then the discrete ordinates approximation will be asymptotically equivalent to a collocation (pseudospectral) discretization of the Fokker-Planck equation. However, this condition is not fulfilled for most standard multidimensional applications with level symmetric quadratures. To fix this problem, Morel[14] suggested the use of an 'exact' Galerkin quadrature and Morel[14] and Reed[16] introduced suitable spherical harmonics interpolation spaces, which are easier to implement in multidimensional problems.

In the remainder of this paper we investigate the use of biased angular quadrature formulas for discrete ordinates numerical calculations of problems with highly forward-peaked scattering. In particular, we investigate the propagation of a particle beam and show that by adopting curvilinear coordinates one can advantageously apply a biased angular formula to best represent the highly anisotropic flux in the local coordinate system. The physics of this problem is discussed in Section 2 where we also introduce a twice-collided correction to help diminish ray effects and to improve the numerical approximation for the residual multiple-collided flux.. In Section 3 we discuss the discrete ordinate approximation and introduce an angular quadrature formula that concentrates the angular directions around the main direction of particle propagation. An important point also discussed here is the angular representation for the source. Since the number of angular flux moments roughly increases with K_{scat}^2 and we are interested in HFPS problems with a high-order of anisotropy, $K_{scat} \sim 10^3$, it is clear that a solution based on a spherical-harmonic

source representation is unfeasible. Instead, we have adopted a storage strategy where angular fluxes, not angular flux moments, are kept for each cell. This implies that our numerical approximation is not subject to compatibility conditions arising from the use of different angular representations and, therefore, our numerical solution unconditionally accepts a Fokker-Planck limit whenever the continuous equation has that limit. However, working with angular fluxes requires the precalculation of an angle-to-angle collision matrix. We show how this matrix can be efficiently calculated and introduce a normalization procedure that complies with particle conservation while respecting the symmetries of the scattering matrix. In the following section we present a numerical discrete ordinates (S_N) solution for the calculation of the transverse spread of a collimated beam in two-dimensional curvilinear cylindrical geometry and discuss our results as well as the shortcomings of this type of calculational procedure. Because of the use of the low-order diamond approximation, and in spite of the tight spatial meshing used in the calculation, we were obliged to introduce a positive fixup that necessarily contaminated the solution. However, the analysis of the results shows promise for the use of biased angular quadratures with more sophisticated spatial discretizations as reference calculations for faster asymptotic methods. Finally, conclusions are given in Section 5.

2. CURVILINEAR COORDINATES

Beam propagation in a medium is described by the following transport equation:

$$\begin{aligned}(\mathbf{\Omega}\cdot\nabla+\Sigma)\psi &= H\psi+\delta_3(\mathbf{r})\delta_2(\mathbf{\Omega}\cdot\mathbf{e}_z),\\ \lim_{|\mathbf{r}|\to\infty}\psi(\mathbf{r},\mathbf{\Omega}) &< \infty,\end{aligned} \tag{4}$$

where $\delta_2(\mathbf{\Omega}\cdot\mathbf{\Omega}')$ is Placzek's delta,[2] $\int d\mathbf{\Omega}'\delta_2(\mathbf{\Omega}\cdot\mathbf{\Omega}')f(\mathbf{\Omega}')=f(\mathbf{\Omega})$, we have considered an infinite geometrical domain and where H is the collision operator in Eq. (3). Because of the structure of the source, the solution for the flux $\psi(\mathbf{r},\mathbf{\Omega})$ from Eq. (4) is invariant under rotations about axis $\mathbf{e}_z$ and also under planar symmetries with respect to planes containing $\mathbf{e}_z$. Under these conditions the size of the problem can be reduced by using a local, position dependent, coordinate frame for the angular direction $\mathbf{\Omega}$. This can be done by writing Eq. (4) in curvilinear cylindrical coordinates with $\mathbf{r}=(z,\rho,\varphi)$ and $\mathbf{\Omega}=(\mu,\phi)$, where z is the axial coordinate, ρ and φ are the polar coordinates on the xy plane, $\mu=\mathbf{\Omega}\cdot\mathbf{e}_z$ is the component of $\mathbf{\Omega}$ along the z axis, and ϕ is the azimuthal angle on the $(\mathbf{e}_\rho,\mathbf{e}_\varphi)$ plane. In these coordinates, the flux reads $\psi(z,\rho,\varphi,\mu,\phi)$. However, because of the symmetry of rotation with respect to the z axis, ψ does not depend on the spatial coordinate φ. Moreover, the planar symmetries with respect to planes containing the z axis makes $\psi(z,\rho,\mu,\phi)$ an even function of the azimuthal angle ϕ, so we only have to consider half of the angular domain, $(\mu,\phi)\in[-1,1]\times[0,\pi]$.

Although the symmetries have eliminated the φ variable and halved the angular domain, in order to solve Eq. (4) in the reduced angular domain one has to replace the scattering operator H with

$$(H_{1/2}f)(\mathbf{r},\mathbf{\Omega})=\int_{(2\pi)}d\mathbf{\Omega}'\Sigma_{s,1/2}(\mathbf{\Omega}'\cdot\mathbf{\Omega})f(\mathbf{r},\mathbf{\Omega}'),$$

where

$$\Sigma_{s,1/2}(\mathbf{\Omega}'\cdot\mathbf{\Omega})=\Sigma_s(\mathbf{\Omega}'\cdot\mathbf{\Omega})+\Sigma_s(s_z\mathbf{\Omega}'\cdot\mathbf{\Omega}),$$

with $s_z\mathbf{\Omega} = (\mu, -\phi)$.

In the next section we present a numerical solution for Eq. (4) based on a discrete ordinates approximation.[17] But, to reduce the concomitant ray effects associated with the presence of localized sources in multidimensional geometries, we write the solution of Eq. (4) as:

$$\psi(\mathbf{r},\mathbf{\Omega}) = \sum_{n=0}^{n=N} \psi_n(\mathbf{r},\mathbf{\Omega}) + \psi_{col}(\mathbf{r},\mathbf{\Omega}),$$

where $\psi_n(\mathbf{r},\mathbf{\Omega})$ is the n-th collided flux and $\psi_{col}(\mathbf{r},\mathbf{\Omega})$ is the solution of the radiative transfer problem with source $(H\psi_N)(\mathbf{r},\mathbf{\Omega})$.[18] In curvilinear cylindrical coordinates the corresponding equation reads:

$$\begin{aligned} &(\mathbf{\Omega}\cdot\nabla + \Sigma)\psi_{col} = H_{1/2}\psi_{col} + H\psi_N \\ &\lim_{|\mathbf{r}|\to\infty} \psi_{col}(\mathbf{r},\mathbf{\Omega}) < \infty \end{aligned} \tag{5}$$

where

$$\mathbf{\Omega}\cdot\nabla \equiv \mu\frac{\partial}{\partial z} + \frac{\eta}{\rho}\frac{\partial}{\partial\rho}\rho - \frac{1}{\rho}\frac{\partial}{\partial\phi}\xi \tag{6}$$

Here $\eta = \mathbf{\Omega}\cdot\mathbf{e}_\rho = \sqrt{1-\mu^2}\cos\phi$ and $\xi = \mathbf{\Omega}\cdot\mathbf{e}_\varphi = \sqrt{1-\mu^2}\sin\phi$ are the components of $\mathbf{\Omega}$ along the $\mathbf{e}_\rho$ and $\mathbf{e}_\varphi$ axes. The third term in the right hand side of Eq. (6) arises from angular redistribution due to the dependence of the angular reference frame on the spatial coordinates.[17]

The singularity of the flux in the beam problem reaches the first-collided component which makes it necessary to regularize the solution with a first-collided correction (N=1). The source $H\psi_1$ in Eq. (5) can be derived from the expression for the first-collided flux. The expressions for the uncollided and first collided fluxes are:[18]

$$\psi_0(\mathbf{r},\mathbf{\Omega}) = \delta_2(\mathbf{\Omega}\cdot\mathbf{e}_r)\frac{e^{-\tau(\mathbf{0},\mathbf{r})}}{r^2}\delta_2(\mathbf{e}_r\cdot\mathbf{e}_z), \tag{7}$$

$$\psi_1(\mathbf{r},\mathbf{\Omega}) = \int_0^\infty dz'\Sigma_s(\mathbf{r}',\mathbf{\Omega}\cdot\mathbf{e}_z)\frac{e^{-\tau(\mathbf{r}',\mathbf{r})}e^{-\tau(\mathbf{0},\mathbf{r}')}}{R^2}\delta_2(\mathbf{\Omega}\cdot\mathbf{\Omega}_R), \tag{8}$$

where $\mathbf{e}_r = \mathbf{r}/r$, $\tau(\mathbf{r}',\mathbf{r})$ denotes the optical distance between the two points, $\mathbf{r}' = z'\mathbf{e}_z$, $\mathbf{R} = \mathbf{r} - \mathbf{r}'$ and $\mathbf{\Omega}_R = \mathbf{R}/R$. In local angular coordinates the delta function in the integrand can be written as $\delta_2(\mathbf{\Omega}\cdot\mathbf{\Omega}_R) = \delta(\phi)\delta(\mu-\mu_R)$ where $\mu_R = (z-z')/R$. Note that the singularity of the first-collided flux originates from the $\delta(\phi)$. Although the delta $\delta(\mu-\mu_R)$ can be eliminated at this stage by integration in z', we prefer to use it later to simplify the calculation of the cell averaged flux.

3. DISCRETE ORDINATES SOLUTION

We have used the discrete ordinates approximation together with diamond interpolation to derive a numerical approximation for the radiative transfer equation in curvilinear cylindrical coordinates. The geometrical domain is a finite cylinder of height z_{max} and radius ρ_{max}. Because of the symmetry of rotation the flux is specified by four coordinates: two spatial coordinates z and ρ and two angular coordinates $\mu = \mathbf{e}_z\cdot\mathbf{\Omega}$ and $\eta = \mathbf{e}_\rho\cdot\mathbf{\Omega}$.

Following the discrete ordinates prescription we consider Eq. (5) for a finite set of prescribed angular directions and use the associated angular quadrature formula to discretize the collision integral. The result is a set of ordinary differential equations coupled through the collision term and well suited for an iterative solution on the scattering source. Spatial discretization is obtained by writing exact cell balance equations in terms of cell and surface mean angular fluxes and by introducing approximate diamond relations across the cell to achieve finite differencing on the spatial variables z and ρ, as well as across the angular cell for the angular variables μ and η.

The use of such a numerical solution for Eq. (5) entails the introduction of approximate boundary conditions at the external surfaces. Because of the localized source and the strongly forward scattering such boundary conditions will not have a significant impact on the solution in the interior of the domain, although the solution will deteriorate near the external boundaries, in particular for negative μ directions for which the flux, anyway, is very small. At the top surface of the cylinder, $z = z_{max}$, we have implemented an asymptotic boundary condition by assuming that the angular flux is in the asymptotic regime and is locally equivalent to the asymptotic flux in slab symmetry.[19] An albedo specular or isotropic boundary condition has been used at the external radial surface of the cylinder, $\rho = \rho_{max}$, with zero albedo or with the albedo obtained from the asymptotic slab geometry regime. This boundary condition also can be used for the other surfaces in both geometries.

In this section we discuss in detail the treatment of the angular variable. Because of the presence of the localized source at the origin of coordinates and the strong anisotropy of scattering the physical picture is that of particles streaming in directions around the uncollided trajectories from the source. In order to construct a good representation of such a strongly anisotropic flux and to achieve a fair calculation of the collision integral we adopt a strongly biased angular quadrature. Moreover, to reduce memory requirements we have decided to store angular fluxes instead of the traditional P_N angular flux moments. We show here how we calculate the associated collision matrix from a point-description of the scattering phase function.

3.1. Angular Quadrature

Because of the invariance with respect to planar symmetries for planes containing $\mathbf{e}_z$ we need only consider half of the angular domain, $(\mu, \phi) \in [-1, 1] \times [0, \pi]$. Also, because of the localized source and the high anisotropy of forward scattering we expect that the flux will be very large for values $\mu \sim 1$ and that it will decrease very fast as μ decreases. For this type of problem the familiar level-symmetric quadrature formulas are inefficient and it is better to adopt a biased angular quadrature formula. We have selected the quadrature

$$\frac{1}{2\pi}\int_{(2\pi)} d\mathbf{\Omega} f(\mathbf{\Omega}) \sim \sum_{p=1}^{N_\mu}\sum_{q=1}^{N_\phi} w_p \overline{w}_q \, f(\mu_p, \phi_q), \tag{9}$$

i.e., a product of a quadrature in μ times a quadrature in ϕ:

$$\frac{1}{2}\int_{-1}^{1} d\mu f(\mu) \sim \sum_{p=1}^{N_\mu} w_p \, f(\mu_p), \quad \frac{1}{\pi}\int_{0}^{\pi} d\phi f(\phi) \sim \sum_{q=1}^{N_\phi} \overline{w}_q \, f(\phi_q).$$

For both formulas, the weights are positive and add up to 1,

$$\sum_p w_p = \sum_q \overline{w}_q = 1. \tag{10}$$

For the ϕ quadrature we have used a uniform formula,

$$\overline{w}_q = \frac{1}{N_\phi}, \quad \phi_q = \frac{\pi}{2N_\phi}(2q-1),$$

which is equivalent to a Gauss-Chebyshev quadrature in η. For the μ quadrature we will introduce a bias by concentrating the μ_p near $\mu = 1$. We also require that both formulas exactly integrate an isotropic angular flux distribution:

$$\sum_{p=1}^{N_\mu} w_p \mu_p = \sum_{q=1}^{N_\phi} \overline{w}_q \, \cos\phi_q = 0. \tag{11}$$

Notice that this constraint is automatically satisfied by the uniform ϕ quadrature.

For our calculations we have used strongly biased polar quadrature formulas with an accumulation of quadrature points near $\mu = 1$. These formulas are defined by subdividing the interval $[-1, 1]$ into N_μ cells with the help of a mesh of the form $\{-1 = \overline{\mu}_0 < \overline{\mu}_1 < ... < \overline{\mu}_{N_\mu} = 1\}$ and by defining the quadrature formula $\{\mu_p, w_p, p = 1, N_\mu\}$ such that

$$\mu_p = \frac{\overline{\mu}_p + \overline{\mu}_{p-1}}{2}, \; w_p = \frac{\overline{\mu}_p - \overline{\mu}_{p-1}}{2}.$$

Obviously this formula satisfies the conditions in Eqs. (10) and (11). It remains to construct an appropriate mesh. With the idea of concentrating the μ quadrature points near the forward direction we start by dividing the basic $[-1, 1]$ interval into two or more subintervals $\{[\overline{\mu}_{i-1}, \overline{\mu}_i], i = 1, N_{sub}\}$.

Next, on each subinterval we use a variable step quadrature to define the final μ cells. If N_i denotes the order of the quadrature in subinterval i, then the cells in that subinterval are obtained using a geometric series of ratio r_i so that each cell has a length r_i times that of the preceding cell. The associated quadrature points and weights are, respectively, the middle points and the lengths of the segments:

$$w_{ik} = r_i^{k-1} w_{i1}, \; \mu_{ik} = \mu_{ik-1} + \frac{w_{i1}}{2} r_i^{k-1}(1 + r_i), \tag{12}$$

where, with $L_i = \overline{\mu}_i - \overline{\mu}_{i-1}$, $w_{i1} = [(1 - r_i)/(1 - r_i^{N_i})]L_i$ and $\mu_{i1} = \overline{\mu}_{i-1} + w_{i1}/2$. Quadrature formulas constructed following these rules integrate exactly the functions 1 and μ. Note that the distances between two consecutive quadrature points $d_{ik} = \mu_{ik} - \mu_{ik-1}$ in a subinterval also form a geometric series of ratio r_i so, for $r_i < 1$, points tend to accumulate toward the end of the subinterval, but their weights may diminish very fast.

3.2. Numerical Representation of Very Forward Peaked Scattering

Highly forward peaked scattering, resulting from electron or photon interactions with matter, is characterized by scale factors of several decades between the backward ($\mu_{coll} = -1$) and the forward directions ($\mu_{coll} = 1$) as well as by a very rapid increase for values close to $\mu_{coll} \approx 1$. The scattering law

can be known from a set of measured values or from an analytical model, such as the Henyey-Greenstein or binomial models. We discuss first the treatment of a scattering function as defined from experimentally measured values.

In practice an experiment would give values of the currents, for a finite set of measurement angles, from a single scattering event as measured by a small aperture detector at each of the measurement angles $\phi = \cos^{-1}\mu_{coll}$. These currents, divided by the area of the detector, provide point values for each measurement angle. Measurements in the purely backward ($\phi = 180$) and forward directions ($\phi = 0$) are especially difficult to perform. In particular, a measurement in the purely forward direction cannot be separated from the uncollided contribution that may introduce a large error. Measured values are given for a set of discrete angles $\{0 < \phi_1 < \cdots < \phi_N = 180\}$ with ϕ_1 typically of the order of 0.1 degrees.[20] Hence, the values of the scattering kernel for small angles have to be obtained from a model or from analytical extrapolation. For photon scattering in sea water, for example, a $\log f_{scat} - \log\phi$ behavior was used[22] to reconstruct the scattering kernel between measurement points as well as to obtain extrapolated values for $\phi < \phi_1$. However, this resulted in an infinite value at the origin so we introduced a lowest $\phi_0 = \epsilon\phi_1$ value, with $\epsilon \ll 1$, and took $f_{scat}(\phi)$ constant in $[0, \phi_0]$ while using the $\log f_{scat} - \log\phi$ interpolation between consecutive points in the grid $\{\phi_i, i = 0, N\}$. The value of $f(\phi_0)$ was iteratively obtained from the normalization condition (1) that, in terms of μ_{coll}, reads:

$$\int_{-1}^{1} d\mu_{coll} f_{scat}(\mu_{coll}) = \frac{1}{2\pi}. \tag{13}$$

This first step is not required when the scattering law is given by an analytical model.

For the calculation of the scattering matrix we have found it expedient to use two constant-step tabulations for $f_{scat}(\mu_{coll})$ in the domains $(0, \mu_{max})$ and $(\mu_{max}, 1)$ and obtain all the required values from linear interpolation in these domains. These tabulations are again renormalized in order to satisfy (13). In our calculations we have used 80000 points for each tabulation with values of μ_{max} of the order of .999, which results in a normalization constant practically equal to unity. The value of μ_{max} is defined so it approximately divides the scattering range into two equal probability domains.

In the case of a scattering law defined from a grid of measured values we use the $\log f_{scat} - \log\phi$ interpolation to construct the tabulations, while for a scattering law defined by an analytical model the tabulated values are obtained from the evaluation of the model at each of the mesh points. However, to avoid any possible divergence for $\mu_{coll} = 1$ we use a constant value in the interval $[\cos\phi_0, 1]$ as defined by $f_{scat}(\cos\phi_0)$.

Finally, the coefficients of the expansion of the scattering kernel on Legendre polynomials, required for the computation of the eigenvalues used in the asymptotic boundary condition, are determined from numerical quadratures.

3.3. Angular Weight Renormalization

The linear tabulation of the scattering kernel has been constructed and renormalized to respect normalization condition (13), $f_0 = 1$. On the other hand, it is essential for overall particle conservation that

the angular quadrature formula should be able to predict the correct value for the mean number of secondaries. This is equivalent to asking that condition (13) be verified when the integral is evaluated using the quadrature formula. Hence, global particle conservation at each collision event will be satisfied if the angular quadrature formula $\{w_p, \mu_p, p = 1, N_\mu\}$ exactly integrates the scattering phase function:

$$2\pi \int_{-1}^{1} d\mu f_{scat}(\mu) \sim 4\pi \sum_{p=1}^{N_\mu} w_p f_{scat}(\mu_p) = 1. \tag{14}$$

To attempt to correctly integrate very highly anisotropic scattering phase functions we use a small value of r_i for the last polar subinterval. But, even though this produces quadrature points very near $\mu_{coll} = 1$, the weights are too small to correctly account for the very rapid rise of $\Sigma_s(\mu_{coll})$ for nearly forward collisions. Therefore we need to introduce a weight renormalization. Because such a renormalization is subject to the three constraints given in Eqs. (10,11,14) we divide the interval $[-1, 1]$ into three subdomains $\{I_i, i = 1$ to $3\}$ and associate a different normalization constant $a_i = 1 + \delta_i$ to each subdomain. Constraints (10) and (11) are used to explicitly compute a_1 and a_2 in terms of δ_3:

$$\begin{pmatrix} a_1 \\ a_2 \end{pmatrix} = \begin{pmatrix} 1 \\ 1 \end{pmatrix} - \frac{\delta_3}{S_1\overline{S}_2 - \overline{S}_1 S_2} \begin{pmatrix} S_3\overline{S}_2 - \overline{S}_3 S_2 \\ S_1\overline{S}_3 - \overline{S}_1 S_3 \end{pmatrix},$$

where

$$S_i = \sum_{k \in I_i} w_k, \ \overline{S}_i = \sum_{k \in I_i} w_k \mu_k.$$

By using these expressions for a_1 and a_2, constraint (14) defines a functional of δ_3 that can be iteratively minimized to obtain the optimal δ_3 value. In our calculations we have defined the last subdomain I_3 as containing only the last μ quadrature point. For the scattering phase functions used for our numerical results this gives a_1 and a_2 very close to 1 and a value for a_3 of the order of 1.2. This means that condition (14) is achieved by increasing the weight of the highest μ quadrature point.

3.4. Computation of the Scattering Matrix

In the discrete ordinates formalism, the angular quadrature is utilized to define the angular directions for which the angular flux is to be calculated and also to construct a numerical approximation of the scattering term $H\psi$. Usually such an approximation is written in terms of angular flux moments, as computed with a spherical harmonic basis. However, for highly anisotropic scattering the number of angular moments can be staggering; for example, for our problem where the angular flux is an even function of ϕ, the number of angular moments is $N_{moments} = (K_{scat} + 1)(K_{scat} + 2)/2$, where K_{scat} is the degree of anisotropy of the scattering phase function when expanded with Legendre polynomials as in Eq. (2).

For scattering in ocean waters such an expansion may require thousands of terms which would demand of the order of millions of angular moments to be kept per geometrical cell in order to compute the scattering source. Therefore, we decided to directly compute the scattering source in terms of the angular flux, which requires storing $N_{angles} = N_\mu N_\phi$ unknowns per cell. However, this approach requires the computation of the associated scattering matrix prior to the calculation of the angular flux. For simplicity we consider the full scattering operator $H$and give later the formula for $H_{1/2}$.

In our treatment we consider the full scattering operator H and give later the formula for $H_{1/2}$. To do this we extend by symmetry about $\phi = \pi$ quadrature formula (9). By integrating the scattering term over the angular domain $(\mu_{p-}, \mu_{p+}) \times (\phi_{q-}, \phi_{q+})$ associated with angular direction $\mathbf{\Omega}_{pq}$=(μ_p, ϕ_q), one may write

$$(H\psi)(\mathbf{\Omega}_{pq}) = \Sigma_s \int_{(4\pi)} f_{scat}(\mathbf{\Omega}'\cdot\mathbf{\Omega}_{pq})\psi(\mathbf{\Omega}')d\mathbf{\Omega}'$$
$$\sim 2\pi\Sigma_s \sum_{p'=1}^{N_\mu}\sum_{q'=1}^{2N_\phi} \langle f_{scat}\rangle_{pq}^{p'q'} w_{p'}\overline{w}_{q'}\,\psi(\mathbf{\Omega}_{p'q'}) = \sum_{p'=1}^{N_\mu}\sum_{q'=1}^{2N_\phi} h_{pq}^{p'q'}\psi(\mathbf{\Omega}_{p'q'}), \tag{15}$$

where $\langle f_{scat}\rangle_{pq}^{p'q'}$ is the mean value of $f_{scat}(\mathbf{\Omega}'\cdot\mathbf{\Omega})$over the angular domains associated with angular directions $\mathbf{\Omega}_{p'q'}$ and $\mathbf{\Omega}_{pq}$, respectively. We calculate this mean value by assuming that the angular flux is constant on each domain:

$$\langle f_{scat}\rangle_{pq}^{p'q'} = \frac{\int_{\mu_{p-}}^{\mu_{p+}} d\mu \int_{\phi_{q-}}^{\phi_{q+}} d\phi \int_{\mu_{p'-}}^{\mu_{p'+}} d\mu' \int_{\phi_{q'-}}^{\phi_{q'+}} d\phi' f_{scat}(\mathbf{\Omega}'\cdot\mathbf{\Omega})}{\int_{\mu_{p-}}^{\mu_{p+}} d\mu \int_{\phi_{q-}}^{\phi_{q+}} d\phi \int_{\mu_{p'-}}^{\mu_{p'+}} d\mu' \int_{\phi_{q'-}}^{\phi_{q'+}} d\phi'}. \tag{16}$$

Also, in order to comply with particle conservation, the $h_{pq}^{p'q'}$, implicitly defined in (15), must satisfy the normalization condition:[21]

$$\Sigma_s = \sum_{p'=1}^{N_\mu}\sum_{q'=1}^{2N_\phi} h_{pq}^{p'q'}. \tag{17}$$

The quantities $\langle f_{scat}\rangle_{pq}^{p'q'}$ are calculated by numerical quadrature and we use the fact that they are symmetric to halve the number of coefficients to be evaluated:

$$\langle f_{scat}\rangle_{pq}^{p'q'} = \langle f_{scat}\rangle_{p'q'}^{pq}. \tag{18}$$

Next, by observing that $\mathbf{\Omega}'\cdot\mathbf{\Omega} = \mu\mu' + \sqrt{1-\mu^2}\sqrt{1-\mu'^2}\cos(\phi'-\phi)$, we eliminate the integration over ϕ by introducing the new variable $\alpha = \phi' - \phi$, and after integration over ϕ we obtain:

$$\langle f_{scat}\rangle_{pq}^{p'q'} = D^{-1}\int_{\mu_{p-}}^{\mu_{p+}} d\mu \int_{\mu_{p'-}}^{\mu_{p'+}} d\mu' \int_{\phi_{q'-}-\phi_{q+}}^{\phi_{q'+}-\phi_{q-}} d\alpha f_{scat}(\mu,\mu',|\alpha|) g_q^{q'}(\alpha) \tag{19}$$

where D is the denominator in Eq. (16) and

$$g_q^{q'}(\alpha) = g_{q'}^{q}(-\alpha) = \min(\phi_{q+}, \phi_{q'+} - \alpha) - \max(\phi_{q-}, \phi_{q'-} - \alpha).$$

A simplification appears for a uniform ϕ mesh where $\phi_{q+} = q\Delta\phi$ and $\phi_{q-} = (q-1)\Delta\phi$ with $\Delta\phi = \pi/N_\phi$. For this case we can write (19) in the following form:

$$\langle f_{scat}\rangle_{pq}^{p'q'} = (\Delta\phi/D)\int_{\mu_{p-}}^{\mu_{p+}} d\mu \int_{\mu_{p'-}}^{\mu_{p'+}} d\mu' \times$$
$$\int_0^1 d\alpha(1-\alpha)[f_{scat}(\mu,\mu',\Delta\phi\,|\alpha+q'-q|) + f_{scat}(\mu,\mu',\Delta\phi\,|\alpha-q'+q|)]. \tag{20}$$

Moreover, since the ϕ mesh is invariant by translation we have the relation

$$\langle f_{scat}\rangle_{pq}^{p'q'} = \langle f_{scat}\rangle_{p1}^{p'|q'-q|+1}, \tag{21}$$

a relation that also applies to the $h_{pq}^{p'q'}$.

We have therefore implemented the following computational strategy: first we compute by numerical quadrature all the $\langle f_{scat}\rangle_{pq}^{p'q'}$ for $q=1$, $p'\leq p$ and for $q'=1,2N_\Phi$; second we use the symmetry condition in Eq. (18) to compute the remaining coefficients for $q=1$ and $p'>p$; third we obtain the $h_{pq}^{p'q'}$ for $q=1$ and normalize them according to relation (17); finally since the directions $\mathbf{\Omega}_{p'q'}$and $\mathbf{\Omega}_{p',2N_\phi+1-q'}$correspond to identical fluxes we use

$$(h_{pq}^{p'q'})_{1/2} = h_{p1}^{p',|q'-q|+1} + h_{p1}^{p',2N_\Phi+2-q'-q},\ 1\leq q,q'\leq N_\Phi$$

to complete the scattering matrix for all values of q. This yields a collision contribution of the form:

$$(H_{1/2}\psi)(\mathbf{\Omega}_{pq}) \sim \sum_{p'=1}^{N_\mu}\sum_{q'=1}^{N_\phi}(h_{pq}^{p'q'})_{1/2}\psi(\mathbf{\Omega}_{p'q'}). \tag{22}$$

For highly peaked scattering $f_{scat}(\mu_{coll})$ is very large for $\mu_{coll}\sim 1$ and decreases very fast for $\mu_{coll}<1$, so in the first step we apply a lower-order quadrature for $\mathbf{\Omega}_{p'q'}\cdot\mathbf{\Omega}_{pq}<1-\varepsilon$, and perform a high-order quadrature only when the cosine of the two angular directions is within ε of 1.

4. NUMERICAL RESULTS

We have calculated the propagation of a beam in a homogeneous medium with a Henyey-Greenstein scattering law,

$$f_{scat}(\mu_{coll}) = \frac{1}{4\pi}\frac{1-g^2}{(1+g^2-2g\mu_{coll})^{3/2}}$$

and a mean scattering cosine of $\overline{\mu}_{coll}=g=0.999$. For this scattering law 99% of the scattered particles are emitted with cosine $\mu_{coll}>0.9945$, of which 94% have $\mu_{coll}>0.9999$, while only 0.02% of the particles are emitted backward, $\mu_{coll}<0$. Although the fraction of backward particles is very small, angular dispersion is much greater in the backward direction than in the forward one: 35% of the backward particles have $\mu_{coll}<-0.5$ against .03% of the forward particles with $\mu_{coll}<0.5$. The other properties of the medium, Σ and c, are those of clear ocean water,[21] $\Sigma=0.151$ m^{-1} and $c=0.24503$. There were two reasons for this small value of the number of secondaries per collision. First, we had already meshed a similar problem in spherical geometry[22] and second, in the absence of acceleration, we wanted to reduce the number of iterations.

To simulate the propagation of a beam in an infinite medium we have adopted a cylinder of height and radius of 10 mean free paths (m.f.p.), corresponding to 66.225 m, with vacuum boundary conditions on the external surfaces and a delta beam of intensity 1 at the center of the bottom surface $z=0$ and in the direction of the z-axis, $S(\mathbf{r},\mathbf{\Omega})=\delta(\mathbf{r})\delta_2(\mathbf{\Omega}\cdot\mathbf{e}_z)$. Uncollided and first-collided fluxes were computed analytically from Eqs. (7) and (8) and the second collided source was then used to obtain a S_N solution for the collided component comprising all particles undergoing two or more collisions.

To perform the calculations we defined geometrical and angular cells by introducing mesh partitions in the coordinates (z,ρ) and (μ,ϕ), respectively, where z and ρ are measured in m.f.p.. For our final calculation

we defined 100 axial and 150 radial cells, providing for a total of 15000 spatial cells, and placed small cells near the origin where the source is located and where we expected a large gradient in z and ρ, and larger cells away from the origin. The width of the axial cells increases by a factor of 1.02382 from one cell to the next, the first cell has a width of 0.025 m.f.p. while the last one has a width of 0.257 m.f.p., while a factor of 1.03317 was used for the radial cells resulting in first and last cells of 0.0025 and 0.3235 m.f.p, respectively. For the angular variables we defined 60 cells of uniform width of 3 degrees for the ϕ variable and 50 cells of increasing widths for the μ coordinate, with a total of 3000 angular cells. The detailed meshes used to define the cells are given in Table 1. The last μ cells were designed to concentrate the quadrature points near $\mu = 1$; as an example we give the last five μ values: 0.999986, 0.999991, 0.999995, 0.999997 and 0.999999.

Table I. Details of the calculation mesh

coordinate	domain	width	number of cells
z (m.f.p.)	$0 \le z \le 10$	$p = 1.02382^a$	100
ρ (m.f.p.)	$0 \le \rho \le 10$	$p = 1.03317$	150
μ	$-1 \le \mu_d \le 0$ $0 \le \mu_d \le 0.85$ $0.85 \le \mu_d \le 1$	$p = 0.963$ $p = 0.965$ $p = 0.7$	9 11 30
ϕ (degrees)	$0 \le \phi_d \le 180$	3.00	60

[a] Intervals change in length from one to the next by a factor of 1.02382.

The total number of unknowns, counting only cell mean fluxes and excluding boundary values, was $15000 \times 3000 = 45,000,000$. The calculation was carried iteratively on the values of the scattering sources. We used four different criteria to determine convergence:

$$\epsilon_1 = \max \left| 1 - \frac{\psi^{new}}{\psi^{old}} \right|, \qquad \epsilon_2 = \max V \left| 1 - \frac{\psi^{new}}{\psi^{old}} \right|,$$

$$\epsilon_3 = \sqrt{\frac{\sum V(\psi^{new} - \psi^{old})^2}{\sum V(\psi^{old})^2}}, \quad \epsilon_4 = \sqrt{\frac{\sum V(1 - \psi^{new}/\psi^{old})^2}{\sum V}},$$

where the maximum values and the sums are done for all (z, ρ, μ, ϕ) spatial and directional cells, V denotes the volume of a cell, and ψ^{new} and ψ^{old} are the new value and the previous value for the mean cell angular fluxes.

An early calculation was run with 100 radial cells and 30 cells in ϕ, resulting in high radial and ϕ gradients and a large proportion of negative fluxes. We decided to increase the number of radial and ϕ cells to those of our final calculation, 150 and 60, respectively. Still, the large number of negative fluxes gave unphysical oscillatory behavior to the solution. At this point we decided to introduce a positive fixup correction. The

final calculation run with this technique was stopped after 27 iterations resulting in the errors $\epsilon_1 = 2.7 \times 10^{-2}$, $\epsilon_2 = 1.1 \times 10^{-4}$, $\epsilon_3 = 3.3 \times 10^{-9}$ and $\epsilon_4 = 1.5 \times 10^{-5}$ with a number of positive fixups of $\sim 13\%$ of the total number of unknowns The average time per iteration was of 8264 s on a one processor of a node of a Compaq alpha server SC ES40/EV70 computer. The time for computing the scattering matrix was 2378 s. The solution had to be computed in several batches, initialized with the previous iterate, and involved a very tedious competitive process with the other users of the machine.

The nature of particle propagation in this problem is conditioned by the highly forward-peaked scattering and by the heavy absorption. First collisions occur at the axis with a rate of $c\exp(-\Sigma z)$. These collisions yield particles with a very forward angular distribution, so most of the particles propagate near the axis with $\mu \sim 1$ and only 0.02% propagate in backward directions, $\mu < 0$. A fraction of 90% of first-collided particles emerging from the axis undergo their first collision within 2.3 m.f.p. of their trajectory. Since most of these particles have $\mu \sim 1$ most of the twice-collided source will appear around the axis with a little bit more spread of angular directions around $\mu = 1$. Besides this twice-collided source concentrated around the axis, a small quantity of twice-collided particles will appear at noticeable distances from the axis; these collisions originate mostly from the small fraction of first-collided particles that are emitted with directions not close to $\mu = 1$ or $\mu = -1$.

It is this twice-collided source that generates the multiple-collided flux solution of the S_N calculation. Because of the large absorption and the highly forward-peaked scattering, a first approximation to this collided flux can be obtained from transport-corrected direct attenuation: this flux decreases exponentially in $\exp[(1-c)\Sigma l]$, where l is the distance along the particle trajectory. In the following we will use the term collided current to designate the current obtained from the S_N calculation comprising all particles that have undergone two or more collisions.

We first examine the global transverse-integrated partial currents. Fig. 1 shows transverse-integrated partial currents for the axial and radial directions versus, respectively, axial and radial distances in m.f.p.. These currents are the total number of particles moving forward of backward across the entire medium, in the axial or in the radial directions, and are defined as

$$J_z^{\pm}(z) = 2\pi \int_0^{\rho_{max}} \rho d\rho J_z^{\pm}(z,\rho),$$
$$J_\rho^{\pm}(\rho) = 2\pi\rho \int_0^{z_{max}} dz J_\rho^{\pm}(z,\rho),$$

and computed at axial and radial cell center coordinates, $\overline{z}_i$ and $\overline{\rho}_j$, as:

$$J_z^{\pm}(\overline{z}_i) \sim 2\pi \sum_j (\rho_{j+1}^2 - \rho_j^2)(J_z^{\pm})_{ij},$$
$$J_\rho^{\pm}(\overline{\rho}_j) \sim 2\pi\overline{\rho}_j \sum_i (z_{i+1} - z_i)(J_\rho^{\pm})_{ij},$$

where $(J_z^{\pm})_{ij}$ and $(J_\rho^{\pm})_{ij}$ are cell-averaged currents computed from numerical angular quadrature over cell averaged fluxes.

Figure 1a depicts the uncollided, first-collided, collided and total forward transverse-integrated axial currents versus axial optical distance. The total current exhibits an asymptotic behavior in $\exp(-.916\Sigma z)$.

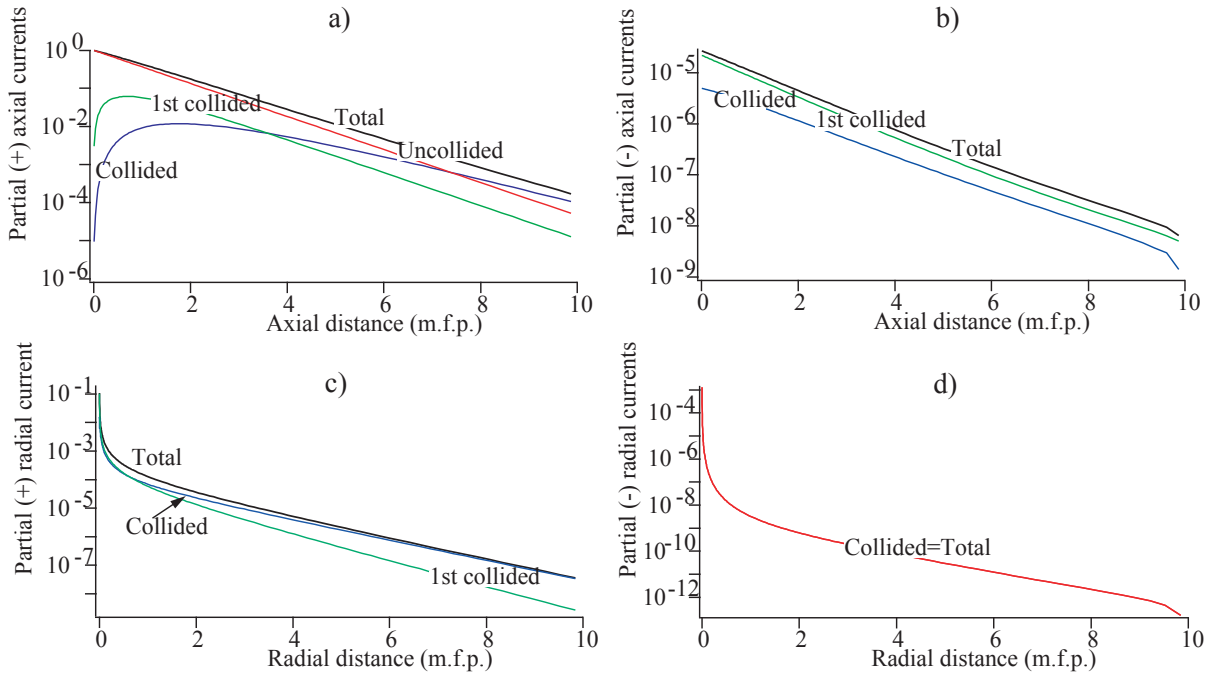

Figure 1. Total transverse-integrated axial currents versus axial cell location and radial currents versus radial cell location: a) axial forward current $J_z^+(z)$, b) axial backward current $J_z^-(z)$, c) radial forward current $J_\rho^+(\rho)$, d) radial backward current $J_\rho^-(\rho)$.

At optical distances greater than 8 m.f.p. the collided current becomes predominant. The first-collided current has a maximum at around 0.71 m.f.p. from the emission point. The collided current exhibits a similar behavior with a maximum around 1.74 m.f.p. These values may be compared to those predicted by a purely forward scattering law with a fraction of forward collisions of c_+. For the latter the first- and second-collided currents are $c_+\Sigma z \exp(-\Sigma z)$ and $(c_+\Sigma z)^2/2 \exp(-\Sigma z)$, with maxima at 1 and 2 m.f.p., respectively, while the maximum of the collided current (two or more collisions) happens at 2.2 m.f.p.. with a value of 1.94×10^{-2}. Clearly the differences shown by the S_N calculation are caused by the angular spreading due to the severe Henyey-Greenstein scattering of the beam.

In contrast, the behaviors of the first-collided, collided and total backwards transverse-integrated axial currents, as shown in Fig. 1b, closely follow an exponential decay, $\exp(-b\Sigma z)$, with coefficients b of -.88 and -.81 and -.91, respectively. Note that the first-collided and second-collided backward currents predicted by a delta forward scattering law from the first backward collided source, $c_-\Sigma \exp(-\Sigma z)$, are $(c_-/2)\exp(-\Sigma z)$ and $(c_-c_+/4)\exp(-\Sigma z)$, while the backward collided current is $(c_-c_+/4)\exp(-\Sigma z)/(1-c_+/2)$. The figure also shows the degradation of the behavior of the currents near the top axial boundary due to the effects of the vacuum boundary condition.

Figures 1c and 1d show the forward and backward radial transverse-integrated partial currents versus radial optical distance. Because of the heavy absorption and of the highly forward scattering these currents are very small except in the immediate vicinity of the beam axis. The total forward radial current in Fig. 1c shows that radial spreading diminishes very rapidly with the distance to the beam axis. The first-collided component is noticeable only very near the axis and disappears fast with radial distance because of the large absorption, while the asymptotic behavior is dominated by the collided current. There is no first-collided contribution to the backward radial current so that the particles heading back have undergone at least two collisions, one along the axis and a second one off axis. As can be seen in Fig. 1d the behavior of the backward radial transverse-integrated current is similar to the forward one with a very fast decrease near the axis followed by an exponential behavior for $\rho > 3$ m.f.p. In this domain the backward radial current behaves as $\exp(-.90\Sigma z)$, while the total forward current behaves as $\exp(-.96\Sigma z)$. Finally, as for the backward axial current, we can also observe a fast decay of the backward radial current near the boundary due to the vacuum boundary condition.

A more detailed analysis of the results can be obtained from cell-averaged axial and radial partial currents, $(J_z^{\pm})_{ij}$ and $(J_\rho^{\pm})_{ij}$, as computed from the angular quadrature of the mean cell fluxes. For the purpose of graphical representation the values of the partial currents are assigned to the centers of the respective cells.

Hereafter we present these currents versus either axial or radial distance at five radial or axial cell

positions, respectively. In the figures we have used the following positions in m.f.p.: ρ equal to 0.00125 (label 1), 0.021 (label 2), 0.062 (label 3), 0.45 (label 4) and 1.24 (label 5) for radial cell positions, and z equal to 0.0125 (label 1), 0.174 (label 2), 0.535 (label 3), 3.21 (label 4) and 7.18 (label 5) for axial cell positions. Notice that the first $\rho = 0.00125$ (label 1) position corresponds to the cells along the axis of the cylinder, whereas the $z = 0.0125$ (label 1) axial position is that of the cells in the bottom of the cylinder. We shall use the notation $J(i, \rho)$ and $J(z, j)$ to denote, respectively, the currents with respect to the radial and axial coordinates, where i and j indicate the label of the respective axial and radial fixed position.

Cell-averaged axial currents $J_z^{\pm}(z, j)$ are represented in Fig. 2a and 2b versus axial location z at the five radial positions. The maxima of the forward currents is the result of competition between the number of (very forward) collisions and absorption. In contrast, except very near the beam axis the backward current always diminishes with axial distance with an exponential behavior in $\sim \exp(-.83\Sigma z)$. This is because for this HFPS medium most of the collided particles heading back have undergone one backward collision followed by one or more forward collisions. For this case the transport-corrected delta scattering predicts a behavior in $(c_- c_+/4)\exp(-\Sigma z)/(1 - c_+/2)$ for the backward current along the axis. The difference with the observed behavior is due to the high angular spreading of the first backward collision together with the dependence on the radial distance.

We discuss now the behavior of the cell-averaged forward and backward axial collided currents $J_z^{\pm}(i, \rho)$ versus radial location ρ, as illustrated in Fig. 2c and 2d at the five axial positions. Although much smaller,

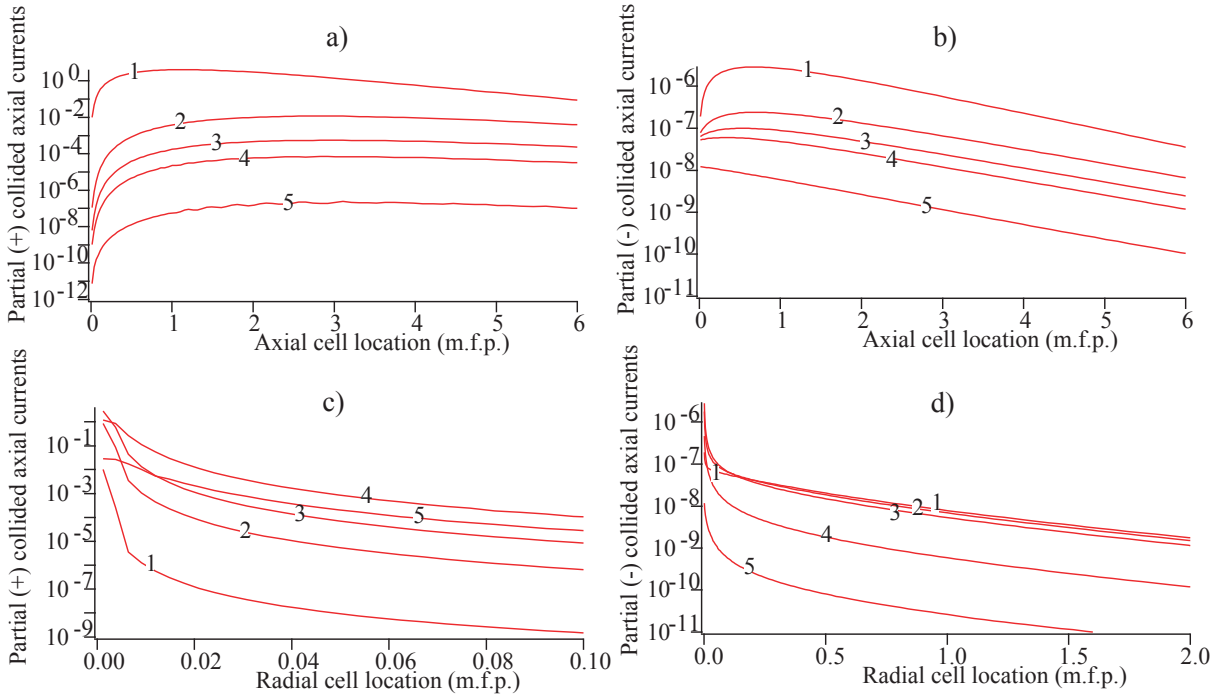

Figure 2. Axial cell-averaged collided currents versus axial cell locations at ρ (m.f.p.) = 0.00125 (j=1), 0.021 (j=2), 0.062 (j=3), 0.45 (j=4) and 1.24 (j=5): a) forward current $J_z^+(z,j)$ and b) backward current $J_z^-(z,j)$; Axial cell-averaged collided currents versus radial cell location at z (m.f.p.) = 0.0125 (i=1), 0.174 (i=2), 0.535 (i=3), 3.21 (i=4) and 7.18 (i=5): c) forward current $J_z^+(i,\rho)$ and d) backward current $J_z^-(i,\rho)$.

the behavior of the backward currents $J_z^-(i,\rho)$ versus radial distance ρ is similar to that of the forward currents $J_z^+(i,\rho)$: a very fast decrease near the origin of the beam, followed by a somewhat slower decay for increasing radial distances. This attests to the fact that the beam remains very close to the beam axis as it propagates along the cylinder. The brusque change in slope of the forward currents is due to the prevalence of second-collision particles near the beam axis.

We examine next the cell-averaged radial currents. Figure 3a and 3b depict the forward and backward radial collided currents $J_\rho^\pm(i,\rho)$ versus radial distance at the five preselected axial locations. Here again we have a competition between absorption and highly forward-peaked scattering. The primary first-collided source decreases exponentially along the axis and with a very small probability sets up a twice-collided source off axis that then propagates collided particles along the radial direction. The attenuation of this propagation with the distance to the axis explains why the radial forward currents decrease with radial distance. Collided particles moving in the radial direction originate from first collisions at the axis, either in the forward or in the backward axial directions. The contribution to the forward radial collided current at

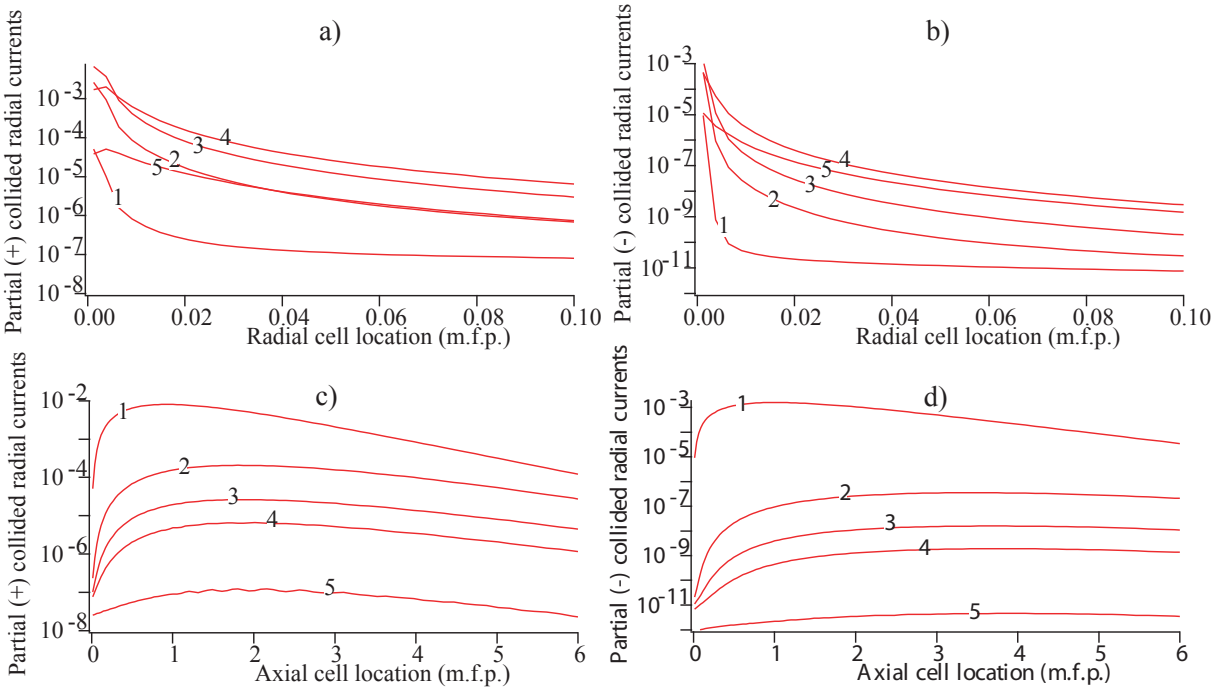

Figure 3. Radial cell-averaged collided currents versus radial cell locations at z (m.f.p.) = 0.0125 (i=1), 0.174 (i=2), 0.535 (i=3), 3.21 (i=4) and 7.18 (i=5): a) forward current $J_\rho^+(i,\rho)$ and b) backward current $J_\rho^-(i,\rho)$; Radial cell-averaged collided currents versus axial cell location at ρ (m.f.p.) = 0.00125 (j=1), 0.021 (j=2), 0.062 (j=3), 0.45 (j=4) and 1.24 (j=5): c) forward current $J_\rho^+(z,j)$ and d) backward current $J_\rho^-(z,j)$.

the bottom axial position (label 1) comes exclusively from backward collisions at the axis. As the axial position increases the contribution of forward scattering at the axis adds a new component to the current that ultimately is damped out as the particles spread out in the radial direction. This explains the maxima observed for the forward radial currents

The behavior of the cell-averaged partial radial currents $J_\rho^\pm(z,j)$ versus axial position is shown in Fig. 3c and 3d for the five radial positions. The maxima exhibited by these currents is determined by two factors: the exponential decrease of the primary first-collided source along the axis and the different contributions of very forward scattering and diffuse scattering. The position of the maximum for the forward currents increases with radial distance because the major part of the current comes from multiple forward collisions with one diffusion collision, either at the axis or at a position off axis. For the backward radial current the main component comes from multiple forward collision ending with a final backward collision. This is the main reason why the maxima are located at greater axial positions.

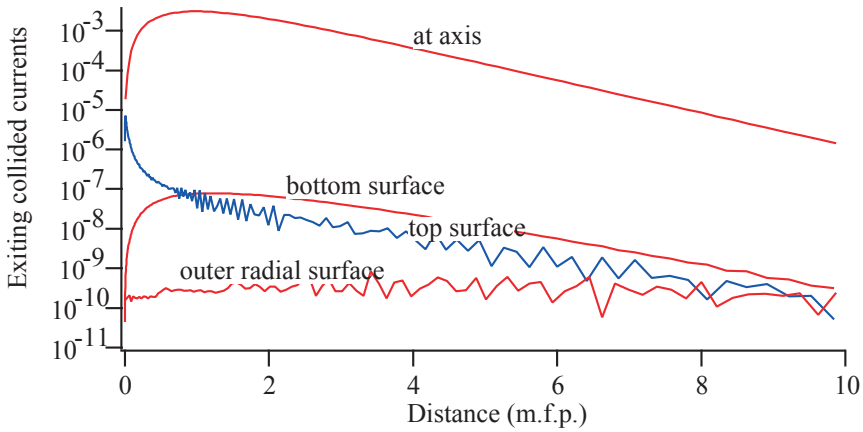

Figure 4. Boundary cell exiting currents versus radial cell position (bottom and top surfaces) and axial cell location (outer radial surface.) The current leaving the axis of the cylinder is also represented.

A final word about the precision of the S_N calculation. The calculation was stopped after 27 iterations because the relative error ε_1 was oscillating about its final value of $\sim 10^{-2}$, while all the other mean errors were stabilized. The oscillations of the relative error ε_1 were induced by the fixup correction and could not be avoided, except by mesh refinement. This of course is the consequence of the low precision of the diamond approximation for a problem with very high flux gradients. With nearly 13% fixups in the last iteration, the results are affected by small local oscillations as seen in the jagged behavior of the cell-averaged currents. This is better illustrated by the exiting currents at the boundary shown in Fig. 4. The oscillations generated by the fixup increase with the distance to the source and are clearly seen in the exiting currents at the top and at the outer radial surface of the cylinder where the size of the cells is much greater than near the locus of the beam at the center of the bottom surface. Because of the vacuum boundary conditions the entering currents are zero. The current leaving the axis of the cylinder is also represented in the figure. Because of the boundary condition at the axis this current equals the current entering the axis.

5. SUMMARY AND CONCLUSIONS

In this work we have analyzed the use of a discrete ordinates numerical method for the calculation of the propagation of a collimated beam in highly forward-peaked scattering (HFPS) media. We have first reviewed different asymptotic approximations that deal with linear transport in HFPS media . An important fact is that the family of Fokker-Plank approximations are not able to cope with some of the scattering models used for HFPS media, in particular with Henyey-Greenstein scattering. Furthermore, none of the asymptotic models provide any useful information for the asymptotic error, and high-order models are very difficult to solve and may result in unstable solutions.

We have considered, therefore, a direct numerical solution of the transport equation. There are two aspects that require special care when using a classical discrete ordinates method for HFPS media. First, the treatment of scattering anisotropy, based on a P_N expansion of the scattering law, requires an extremely high number of terms and demands a prohibitive amount of memory for the storage of cell flux moments. Second, the use of level-symmetric quadrature formulas is not well adapted to the highly anisotropic angular flux characteristic of the propagation of a particle beam in a HFPS medium.

To circumvent these limitations we have decided to store cell-averaged angular fluxes for all angular directions and to use a strongly biased angular quadrature formula. In turn, the use of cell-averaged angular fluxes entails the precalculation of an angle-to-angle scattering matrix. Since the novelty aspects of this problem have to do with the angular discretization and with the angular source representation we have focused only on those aspects of the discrete ordinates approximation that have to do with the angular discretization and not on those that are related to the spatial discretization. For the latter we decided to use the familiar diamond approximation.

To simulate the propagation of a collimated beam in an infinite medium we have considered a homogeneous cylinder of large optical dimensions with nonreentrant boundary conditions and with a beam of unit intensity normally impinging on the center of the bottom surface. In order to reduce the number of unknowns we used axial symmetry of the problem to write the transport equation in two-dimensional curvilinear cylindrical coordinates. Since we expected the flux to be very much concentrated around the axial direction we have adopted a polar angular quadrature formula that concentrates the angular directions $\mathbf{\Omega}$ near $\mathbf{e}_z$, where $\mathbf{e}_z$ is the unit vector in the direction of the axis of the cylinder. Clearly, most of the particles will spread around the axis under the action of very forward collisions and, as they progress along the cylinder, the particles will concentrate around directions $\mathbf{\Omega}$ with decreasing cosines $\mathbf{\Omega} \cdot \mathbf{e}_z$ so that the biased polar angular quadrature, that has been tailored around $\mathbf{\Omega} \cdot \mathbf{e}_z = 1$, will be less efficient. But this will happen after many collisions and therefore at large axial optical positions.

In order to reduce the singularity of the computed angular flux and increase the accuracy of the numerical discretization we have used an analytically calculated twice-collided source. This is necessary because the first collided source for the beam problem contains a singularity in $\delta(\phi)$, where ϕ is the azimuthal angle in the local reference frame. We have written a trial FORTRAN90 computer program based on discrete ordinates and the diamond approximation to compute the angular flux produced by the twice-collided source created by the beam. In this code the source is computed from the cell-averaged angular fluxes. Another version of the code, written for the two-dimensional curvilinear spherical coordinates has been used for a companion paper.[22]

In order to deal with the very strong gradients resulting from the collimated beam propagation in a HFPS medium we have used a nonuniform spatial mesh that concentrates the cells both near the axis and near the bottom of the cylinder. Also, to account for the HFPS we have used a strongly biased polar angular

quadrature, while a uniform angular quadrature has been used for the azimuthal angle. Finally, in order to minimize the number of costly source iterations, we have run the calculations for a very absorbent medium with a number of secondaries per collision $c = .24503$. This value is that of clear ocean water that was also used in some of the calculations in spherical geometry presented in our companion paper.

Our trial calculations showed that even with a large number of spatial and angular cells there was a sizable proportion of negative fluxes. To avoid this unphysical result we have run our final calculation by introducing a positive fixup correction. We have presented a number of results for transverse-integrated and for cell-averaged axial and radial partial currents. The results illustrate the very small radial spread of the beam as it progresses along the axis of the cylinder.

The results and the methodology used in the calculations call for some comments. First of all, it is clear that the use of a diamond discretization is a very poor choice for these problems. Although this was evident at the beginning of our research, our purpose in this work was to explore the feasibility of a numerical solution of the transport equation and to analyze exclusively the details of the angular treatment. We believe that these points have been demonstrated. Accurate discretization schemes such as finite elements or linear discontinuous approximations are well understood and are currently used to the treatment of HFPS problems.[23] However, to our knowledge such approximations have not been applied in the context of a curvilinear coordinates representation of the transport equation. We hope that the present work will stimulate workers in this area to develop such schemes in complicated multidimensional geometries. Second, although some problems, such as the one investigated here of photon propagation in ocean waters, have very high absorption and do not require acceleration of the source iterations, most of the applications to charged particle transport, in particular in the biomedical arena, have very small absorption. For these problems an iterative numerical solution on the scattering source, either by a Monte Carlo or deterministic approach, is terribly expensive without an efficient acceleration procedure. In spite of some progress recently achieved in this area,[24]−[26],[27] this remains the main cornerstone for the realization of efficient computational methods for HFPS problems. Finally, the use of a uniform quadrature for the azimuthal angular coordinate is appropriate for this problem because the first-collided flux has a discontinuity in $\delta(\phi)$ and most of the twice-collided source is produced very near the axis from particles with $\phi \sim 0$. Thus, the biased polar and the uniform azimuthal angular quadratures are well suited for collisions from particles with directions $\mathbf{\Omega}$ near $\mathbf{e}_z$ which, for the problem treated here, account for most of the collisions. Precision on the angular quadrature diminishes for collisions originated from the particles that leave the axis or propagate with a sizable radial component of the angular direction. However the proportion of these particles is very small and therefore the loss of precision is not important.

Since most of the particles originating from the twice-collided source propagate nearly in the direction of emission, a way to improve the accuracy of the solution would be to use a forward delta-scattering approximation $\psi_{col} = \psi_f + \psi_d$, where ψ_{col} is the flux created by the twice-collided source S_2 and ψ_f is the

transport-corrected flux solution of

$$[\mathbf{\Omega}\cdot\nabla+\Sigma(1-c_+)]\psi_f = S_2,$$
$$\lim_{|\mathbf{r}|\to\infty}\psi_f(\mathbf{r},\mathbf{\Omega})<\infty.$$

Here $c_+\sim c$ should account for most of the particles heading in nearly straight directions. This flux can be determined analytically and then one would have to compute numerically the diffuse component ψ_d by solving the transport equation

$$(\mathbf{\Omega}\cdot\nabla+\Sigma)\psi_d = H\psi_d + S_{d2},$$
$$\lim_{|\mathbf{r}|\to\infty}\psi_d(\mathbf{r},\mathbf{\Omega})<\infty$$

with the source $S_{d2}=H\psi_f-\Sigma c_+\psi_f$. However, a potential problem with this approach is that the source S_{d2} is not positive in the forward direction.

Another point has to do with the calculation of the angle-to-angle collision matrix. Because of the HFPS this calculation requires a very accurate numerical quadrature and, therefore, is numerically expensive. We have taken advantage of the uniform azimuthal angular quadrature to reduce the computing time but, nevertheless, the time required for the evaluation of this matrix was nearly one third of the time needed for a source iteration with positive fixup. This implies that the evaluation of the scattering matrix in a multigroup calculation will require not only a large amount of storage memory but also a sizable amount of computing time.

The cost of each source iteration and the large number of iterations that would be necessary for a HFPS with small absorption, as is the case for electron transport, would make this type of direct solution prohibitive except if an acceleration scheme is implemented. Nevertheless, even a few-scattered solution remains a viable source of reference calculations that could be used to check the accuracy of less expensive asymptotic approximations.

In summary, in this work we have shown that the use of biased angular quadratures in conjunction with an angular flux representation shows promise for the discrete ordinates solution of highly forward-peaked scattering problems. However, a drawback of such formulas is that they have to be tailored to the problem at hand. A more flexible approach could consist of a domain partition with local angular representations adapted to the behavior of the flux in each subdomain. We believe that the development of a discrete ordinates code based on biased angular representations and on an accurate spatial approximation could provide reference calculations for faster, asymptotic approximations of the transport equation such as those reviewed in the Introduction. However, a main requirement for practical applications remains the development of appropriate acceleration schemes for the inner iterations. The advantage of a direct numerical solution is that it provides a complete flux map for the domain under analysis. We believe that the use of accurate spatial discretizations and the implementation of an acceleration scheme would make this type of direct numerical solution attractive as compared to a Monte Carlo calculation.

ACKNOWLEDGEMENTS

The authors are grateful to Anna K. for her help with the figures. The final calculations were run on the CEA (Commissariat à l'Energie Atomique) computers at Grenoble. Special thanks are do to Igor Zmijarevic for his help with the use of the Compac alpha server. This work was partially supported by the U.S. Office of Naval Research.

REFERENCES

[1] B. Rossi and K. Greisen,"Cosmic Ray Theory," *Rev. Mod. Phys.*, **13**, 265, 1941.

[2] K.M. Case, F. de Hoffmann and G. Placzek, *Introduction to the theory of neutron diffusion*, U.S. Government Printing Office, Washington, D.C., 1953.

[3] S. Chandrasekhar, "Stochastic Problems in Physics and Astronomy," *Rev. Modern Phys*., **15**, 1-89, 1943.

[4] G.C. Pomraning, "The Fokker-Planck Operator as an Asymptotic Limit," *Math. Models Meth. Appl. Sci*., **2**, 21-36, 1992.

[5] L.G. Henyey and J.L. Greenstein, "Diffusive Radiation in the Galaxy," *Astrophys. J.*, **93**, 70, 1941.

[6] C. Börgers and E.W. Larsen, "On the Accuracy of the Fokker-Planck and Fermi Pencil Beam Equations for Charged Particle Transport," *Med. Phys*., **23** (10), 1749-1759, 1996.

[7] G.C. Pomraning, "A Non-Gaussian Treatment of Radiation Pencil Beams," *Nucl. Sci. Eng*. **127**, 182-198, 1997.

[8] G.C. Pomraning and A.K. Prinja, "The Pencil Beam Problem for Screened Rutherford Scattering," *Nucl. Sci. Eng.*, **130**, 1-17, 1998.

[9] G.C. Pomraning , "The Transport Theory of Beams," *Trans. Th. Statist. Phys.* **29**, 1-41, 2000.

[10] G.C. Pomraning, "Higher Order Fokker-Planck Transport Operators," *Nucl. Sci. Eng*. **124**, 390, 1996.

[11] C.L. Leakeas and E.W. Larsen, "Generalized Fokker-Planck Approximations of Particle Transport with Highly Forward-Peaked Scattering," *Nucl. Sci. Eng.*, **137**, 236-250, 2001.

[12] J.E. Morel, "Fokker-Planck Calculations Using Standard Discrete Ordinates Transport Codes," *Nucl. Sci. Eng.*, **79**, 340, 1981.

[13] J.E. Morel, "An Improved Fokker-Planck Angular Differencing Scheme," *Nucl. Sci. Eng.*, **89**, 131, 1985.

[14] J.E. Morel, "Hybrid Collocation-Galerkin-S_N Method for Solving the Boltzmann Transport Equation," *Nucl. Sci. Eng.*, **101**, 72, 1989.

[15] S.D. Pautz and M.L. Adams, "An Asymptotic Study of Discretized Transport Equations in the Fokker-Planck Limit," ANS Int. Top. Mtg. on Mathematics and Computations, Reactor Physics and Environmental Analysis in Nuclear Applications, M & C ' 99, Madrid, Spain,, Vol. 1, 647-656, 1999.

[16] W.H. Reed, "Spherical Harmonics Solutions of the Neutral Transport Equation from Discrete Ordinate Codes," *Nucl. Sci. Eng*., **49**, 10, 1972.

[17] J.J. Duderstadt and W.R. Martin, *Transport Theory*, Wiley, New York, 1979.

[18] R. Sanchez, "On the singular structure of the uncollided and first-collided components of the Green's function," *Ann. Nucl. Energy*, **27**, 1167-1186, 2000.

[19] K.M. Case and P.F. Zweifel, *Linear Transport Theory*, Addison-Wesley, Reading, MA, 1967.

[20] T.J. Petzold, "Volume Scattering Functions for Selected Ocean Waters," Scripps Institution of Oceanography (La Jolla, Calif.), Ref. No. 72-78, pp. 1-78, 1972.

[21] C.D. Mobley, *Light and Water: Radiative Transfer in Natural Waters*, Academic Press New York, 1994.

[22] R. Sanchez and N.J. McCormick, "Analytic Beam Spread Function for Ocean Optics Applications," *Appl. Opt.*, **41**, 30, 6276-6288, 2002.

[23] L.J. Lorence, Jr., J.E. Morel and G.D. Valdez, "User's Guide to CEPHX-ONELD: A One-Dimensional Coupled Electron-Photon Discrete Ordinates Code Package," SAND 89-1661, Sandia National Laboratories, 1989.

[24] J.E. Morel and T.A. Manteuffel, "An Angular Multigrid Acceleration Technique for S_N Equations with Highly Forward-Peaking Scattering," *Nucl. Sci. Eng.*, **107**, 330, 1991.

[25] S.D. Pautz, J.E. Morel and M.L. Adams, "An Angular Multigrid Acceleration Method for S_N Equations with Highly Forward-Peaking Scattering," ANS Int. Top. Mtg. on Mathematics and Computations, Reactor Physics and Environmental Analysis in Nuclear Applications," M & C ' 99, Madrid, Spain,, Vol. 1, 647-656, 1999.

[26] M.L. Adams and T.A.Wareing, "Diffusion-Synthetic Acceleration Given Anisotropic Scattering, General Quadratures and Multidimensions," *Trans. Am. Nuc. Soc.*, **68**, 203-204, 1993.

[27] D.R. Tolar, Jr. and E.W. Larsen, "A Transport Condensed History Algorithm for Electron Monte Carlo Simulations," *Nucl. Sci. Eng.*, **139**, 47-65, 2001.